Self-Assembly of π-Conjugated Amphiphiles: Free Standing, Ordered Sheets with Enhanced Mobility

Bhawani Narayan, Satyaprasad P. Senanayak, Ankit Jain, K. S. Narayan, and Subi J. George**

Oligo(*p*-phenylenevinylenes) (OPVs) with amphiphilic character are synthesized and their self-assembly characteristics studied. Careful studies point at two morphologically different states of assemblies, with one being two dimensional sheets and the other as rolled tubes. This is also the first time that self-assembled sheets are achieved for OPVs. Morphological and photophysical studies reveal a unique aggregate to aggregate transition between rolled tubes and two dimensional sheets, which is outlined as a more thermodynamic aggregate. The thermodynamic aggregate (2D sheet) is better ordered and consists of chromophores that are better excitonically coupled. The mobilities of these aggregates are also studied for a field effect transistor device and as expected sheets supersede rolled tubes by a couple of orders. More interestingly, the mobility values obtained for the well ordered chromophores in sheets is three orders higher than any other self-assembled OPV previously reported. It is hypothesized that the better π interactions enforced by the amphiphilic design and the resultant supramolecular organization is a prime factor for such a remarkable rise in mobilities.

1. Introduction

Supramolecular ordering of π-conjugated molecules plays a vital role in the performance of organic opto-electronic devices.[1] Controlling the morphologies at the nanometer-scale in solution processable polymers during its fabrication via spin-coating is challenging due to their structural defects.[2] In this respect, the self-assembly of π-conjugated oligomers, with well-defined chemical structure,[3] in solution using supramolecular design principles,[4] has attracted immense attention as it allows enhanced structural control over the organization and functional properties. However, the electroactive devices fabricated from self-assembled π-conjugated oligomers have often showed poor performance[5] compared to highly organized assemblies of less processable counterparts, in the crystal and vacuum deposited thin film states.[6] One of the reasons for low efficiencies in supramolecular chromophoric systems could be the molecular design with solubilizing side chains, which hamper the molecular order and disrupt the extended π–π stacking in the assemblies. In this regard, an amphiphilic design for self-assembly of chromophores can be of particular interest.[7] Moreover, it has been shown that hydrophobic interactions between the amphiphilic systems can give rise to less dynamic assemblies with high association constants.[8] Hence, we envisage that an amphiphilic design combined with the electroactive chromophore can give rise to highly ordered assemblies with stronger π–π interactions and hence better mobilities.

Oligo(*p*-phenylenevinylene)s (OPVs) have been the subject of intense research in the field of organic electronics[3,9] primarily because of the properties exhibited by their polymeric counterparts (PPVs).[10] A variety of supramolecular nano-architectures have been constructed, by the self-assembly of OPV donor molecules in solution,[11] however the hole transport properties of these assemblies are much lower compared[12] to other self-assembled electroactive counterparts.[5a,13] On the other hand, significantly high mobilities have been achieved for less processable OPV counterparts, when they were vacuum deposited as thin film states.[6c] Hence we have selected OPV backbone as a model system to study the effect of amphiphilic substitution and subsequent molecular ordering on the electronic properties of self-assembled chromophoric systems.

Herein, we report the 2D self-organization of amphiphilic oligo(*p*-phenylenevinylene)s, which form free-standing sheets[14] with highly ordered bilayers and hence enhanced mobility. Although, OPV amphiphilic assemblies have been achieved in solution and liquid crystalline phases,[15] they have not yet been investigated for their electronic performances. In addition, this is the first report of 2-D organization of OPVs into sheets by a solution-state self-assembly. We further show an unprecedented, solvent dependent phase transition of these 2-D sheets to scrolled nanotubes. Chiroptical probing

B. Narayan, A. Jain, Dr. S. J. George
Supramolecular Chemistry Laboratory
New Chemistry Unit
Jawaharlal Nehru Centre for
Advanced Scientific Research (JNCASR)
Jakkur P.O., Bangalore 560064, India
E-mail: george@jncasr.ac.in
S. P. Senanayak, Prof. K. S. Narayan
Molecular Electronics Lab
Chemistry and Physics of Materials Unit
JNCASR, Bangalore 560064, India
E-mail: narayan@jncasr.ac.in

DOI: 10.1002/adfm.201202298

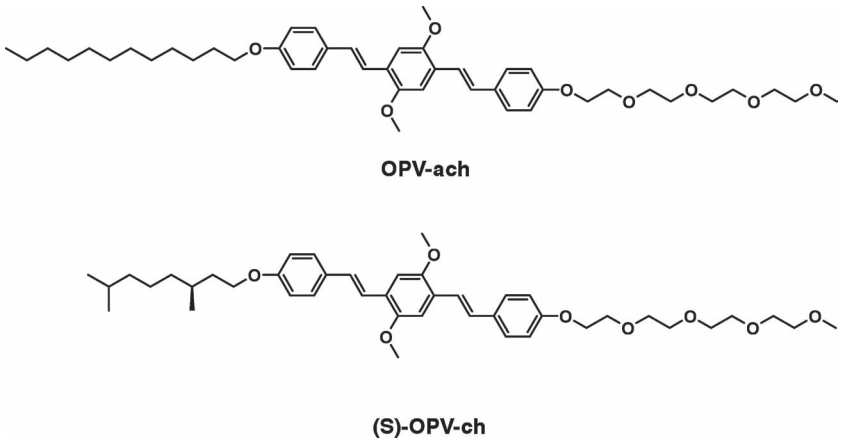

Scheme 1. Molecular structures of **OPV-ach** and **(S)-OPV-ch**.

of the self-assembled sheets further provided insights into the molecular organization and revealed a highly cooperative and reversible temperature dependent phase transition to less ordered assemblies. More importantly, the OPV sheets showed mobilities up to 0.8×10^{-2} cm^2 V^{-1} s^{-1}, which is many orders of magnitude greater than the reported values for the self-assemblies of OPVs and few other well-studied chromophores on a device structure.[5a,12] Recently, Pei et al. have shown that an amphiphilic design for chromophores can indeed result in high mobility self-assembled films.[14b] The mobility magnitude obtained in our system is only about an order of magnitude lower than the values obtained for vacuum-deposited OPV films[6c] and comparable to the recently reported amphiphilic chromophoric self-assembly, reiterating the importance of an amphiphilic design.[14b]

2. Results and Discussion

2.1. Design and Synthesis

Scheme 1 shows the molecular structures of the OPV amphiphiles, **OPV-ach** and **(S)-OPV-ch**, under study. These molecules have a rod-coil structure, with the conjugated back-bone forming the rigid part and the hydrophilic tetraethylene glycol (TEG) chain and hydrophobic dodecyl (for **OPV-ach**) or (S)-citronellyl (for **(S)-OPV-ch**) on the opposite sides constituting the coil. The OPV amphiphiles were synthesized through a statistical Wittig–Horner reaction and have been fully characterized by nuclear magnetic resonance (NMR) spectroscopy, matrix-assisted laser desorption/ionization time-of-flight (MALDI-TOF) and high-resolution mass spectrometry.[16]

2.2. Self-Assembly of OPV Amphiphiles

The self-assembly of **OPV-ach** and **(S)-OPV-ch** was studied in varying ratios of THF-water solvent mixtures and has been probed by various microscopic, light-scattering and spectroscopic techniques.

2.2.1. Microscopic Probing of the OPV Self-Assemblies

Atomic force microscopy (AFM) studies of **OPV-ach** (2.5% THF in water) showed the presence of large sheets of 5–50 μm width suggesting a 2D self-assembly (**Figure 1**a). AFM height profile analysis clearly showed the presence of multiple layers in the sheets. The individual sheets with height close to the amphiphilic bilayer distance were obtained through a height profile analysis of tapping mode AFM images (Figure 1a).[16] The free-floating nature of the sheets in solution is evident from the confocal fluorescence microscopy studies. Bright green fluorescent sheets were observed when a solution of **OPV-ach**, sealed between glass slides was imaged at an excitation of 458 nm (Figure 1b). The presence of wrinkled and folded sheets in the confocal images demonstrates the free-standing nature of the sheets, indicating that the 2D self-assembly indeed occurred in the solution and not due to any dewetting process on the substrates. Transmission electron microscopy (TEM) studies revealed unprecedented details into the structural organization of the bilayers in the OPV sheets (Figure 1c,d).[16] Imaging of the standing edges of the sheets, which were stained with uranyl acetate on a carbon coated copper grid, clearly showed highly ordered molecular arrangement along their sliding edges (Figure 1c). This is further evident from the TEM image in Figure 1d, which provides a cross- sectional view of partially folded multi-layer sheets. The measured periodic distance between stacked sheets from the TEM electron density profile is 4.6 nm, which matches with the OPV bilayer distance, in which the hydrophobic dodecyl chains are completely interdigitated and tilted (Figure 1e). This indicates that the edges of the sheets consist of bilayers with the OPV backbones vertically oriented and the π-stacking direction along the plane of the sheets as reported in literature.[14b] X-ray diffraction (XRD) studies performed on these sheets exhibited d-spacing of 4.4 nm that may be attributed to the tilted, interdigitated bilayer distance and also show higher order reflections characteristic of the lamellar organization.[16]

Remarkably, the planar sheets of **OPV-ach** roll-up into 1D nanotubular structures at high percentages of THF (Figure 1f,g). Confocal images of **OPV-ach** in 20% THF-water solvent mixture revealed the formation of 1D structures (Figure 1f).[16] FE-SEM images revealed the tubular nature of these structures with several micrometers length and an average diameter of 300 nm. Careful analyses of the FE-SEM images showed that these nanotubes are indeed formed by the rolling of the 2D sheets (Figure 1g, insets). TEM of the tubular bundles stained with uranyl acetate revealed randomly oriented bilayers, which could be due to the irregular folding of multiple sheets.[16] The less molecular ordering in the nanotubes was evident from a thin film XRD which revealed multiple peaks whereas XRD of sheets had only two peaks, suggesting more symmetry and higher ordering between the chromophores.[16] Self-assembled organic nanotubes of amphiphilic molecules are generally formed through the coiling of twisted 1D nanotapes[17] or by the

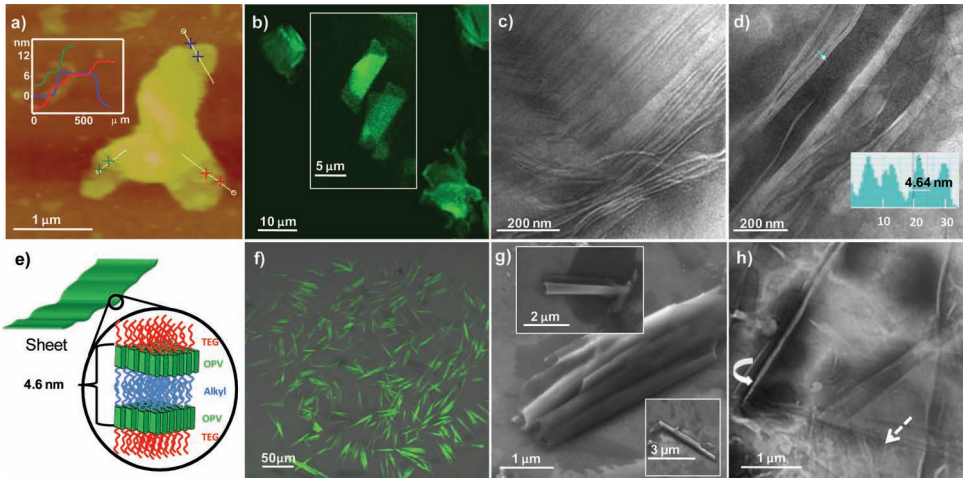

Figure 1. Morphology of the self-assembled OPVs from various THF/water solvent mixtures. a-d) Show the microscopic images of the **OPV-ach** sheets in 2.5% THF in water. a) Tapping mode AFM of a partially folded sheet. Inset shows the height profile across the folding edges, as marked by corresponding colored lines in the figure, showing typical bilayer distances. The bilayers are clearly evident from the step profiles in height analyses. b) Confocal microscopy images (λ_{exc} = 458 nm) showing free-standing green fluorescent sheets in solution. c) TEM image of the sheets viewed along their edges showing the bilayer arrangement, d) TEM image of a partially folded, multi-layered sheet along with the electron density profile of the layers (inset, marked as white bar in the image). e) Schematic representation of the molecular organization in the sheets. f) Confocal (λ_{exc} = 458 nm) and g) FE-SEM images of the **OPV-ach** rolled nanotubes in 20% THF in water. h) TEM image of **(S)-OPV-ch** showing stacked sheets scrolling at the edges formed in 2.5% THF in water (dotted lines and arrows inserted to guide the eye).

rolling-up (scrolling)[18,14a] of 2D nanosheets. Although there are many examples in literature for coiled nanotubes, rolled-up nanotubes are seldom reported. It has been predicted and experimentally shown that self-assembled 2D sheets exhibit a high-temperature rolled-up tubular phase.[19,14a] Here, we observe that, this rolled-up tubular phase can also be attained by varying the solvent compositions. It is noteworthy that **(S)-OPV-ch** also exhibits two types of assemblies with different morphologies and optical properties in water-THF solvent mixtures, similar to its achiral analogue (Figure 1h).[16]

2.2.2. Dynamic Light-Scattering Studies

Dynamic light scattering studies (DLS) on the **OPV-ach** and **(S)-OPV-ch** amphiphiles in THF-water mixtures further supported the fact that not only these assemblies are formed in solution but they are also dependent on the solvent compositions. In 2.5% THF-water solvent mixtures, **OPV-ach** exhibited large polydisperse aggregates with an average hydrodynamic radius of 1000 nm, consistent with the 2D sheets.[16] However, the increase in THF composition resulted in a decrease in the average hydrodynamic diameter (122 nm, 20% THF in water) with much narrower distribution, reiterating the formation of tubular objects from the rolling of sheets. In this report, nanosheet assemblies would be further referred to as State A and the nanotube assembled state as State B. Similarly, DLS studies of **(S)-OPV-ch**, showed aggregates of 1000 and 120 nm, corresponding to the State A (2.5% THF) and State-B (10% THF), respectively (**Figure 2**a).

2.2.3. Spectroscopic Probing of the OPV Self-Assemblies

Detailed optical studies of the two states of OPV amphiphilic self-assembly, further revealed the intermolecular interactions between OPV chromophores[11] with distinct spectroscopic signatures suggesting different molecular organizations. In **OPV-ach**, nanosheets can be characterized by the presence of a vibronic shoulder band at 440 nm in the absorption spectrum, which is in accord with literature reports for OPV intermolecular excitonic interactions[11] and the appearance of red shifted emission bands with maxima at 503 and 540 nm, compared to the monomer emission at 441 and 465 nm (Figure 2b,c). Notably, the red-shifted vibronic absorption band characteristic of strongly π-stacked OPV chromophores is absent for the nanotubes, although the self-assembly is marked by its red-shifted emission bands at 491 and 525 nm. These optical changes are characteristic of the J-type molecular ordering of the OPV chromophores,[11c,d] which is further confirmed by excitation spectra and time-resolved fluorescence studies.[16] Excitation spectra collected at 550 nm emission wavelength for State A showed the vibronic shoulder at 440 nm similar to the self-assembled absorption spectrum. Time resolved fluorescence measurements clearly indicate that the lifetime of the aggregate in 2.5% THF in water (τ_1 = 1.92 ns (84.3%), τ_2 = 3.8 ns (15.7%) is higher than the monomer (1.53 ns), hence indicating a J-type aggregate.[16] These measurements along with the front-face emission measurements clearly rule out the other possibilities of self-absorption and energy transfer for the fluorescence quenching of monomer.[16] We have further studied the self-assembly of **(S)-OPV-ch**, bearing a chiral side chain, to obtain a detailed understanding of the packing of chromophores in the two different kinds of assemblies, using chiroptical properties as a probe. Absorption and emission studies of **(S)-OPV-ch** showed similar changes as that of its achiral analogue for both states.[16] Remarkably, circular dichroism (CD) studies performed on State B showed that these assemblies are CD silent, while State A is marked by the appearance of a bisignated CD signal with the positive maximum at 415 nm and the negative

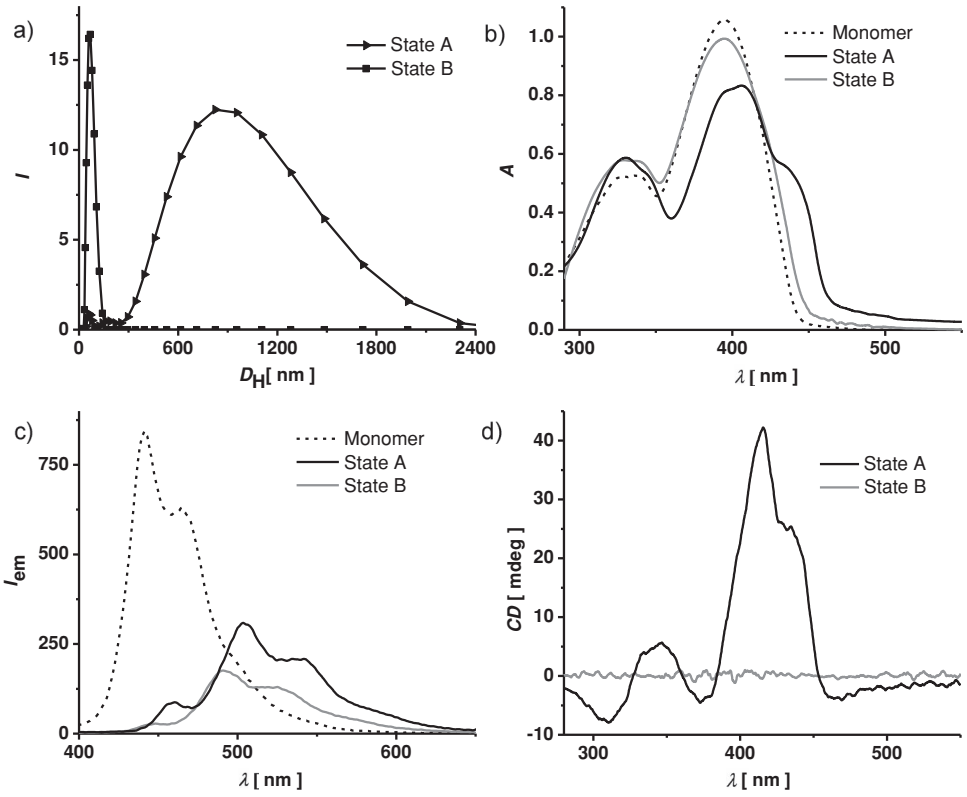

Figure 2. Characterization of the State A and State B phases in OPV amphiphiles: a) aggregate size changes monitored by DLS in **(S)-OPV-ch** ($c = 5 \times 10^{-5}$ M), b) absorption and c) emission spectra of **OPV-ach** ($c = 2.5 \times 10^{-5}$ M, $\lambda_{exc} = 380$ nm, l = 10 mm). d) CD spectra of the two states in **(S)-OPV-ch** ($c = 5 \times 10^{-5}$ M).

maximum at 375 nm[16] characteristic of excitonically coupled OPV chromophores (Figure 2d).

2.2.4. Phase Transitions

Notably, in the present case, temperature dependent chiroptical studies of **(S)-OPV-ch** in State B have shown that an annealing process can improve the molecular ordering in the assemblies and the tubes can be converted to the nanosheets (similar to State A), suggesting that State A is a more thermodynamically favorable phase.[17] CD cooling experiment of state B (10% THF in water, 5×10^{-5} M) at the rate of 2 °C/min monitored at 415 nm, showed a sudden appearance of the bisignated CD signal below 22 °C, characteristic of excitonically coupled chromophores (**Figure 3**a). The development of a bisignated CD signal with annealing is corroborated by the appearance of a vibronic shoulder at 440 nm in the absorption spectrum similar to that of State A.[16] Interestingly, the hydrodynamic

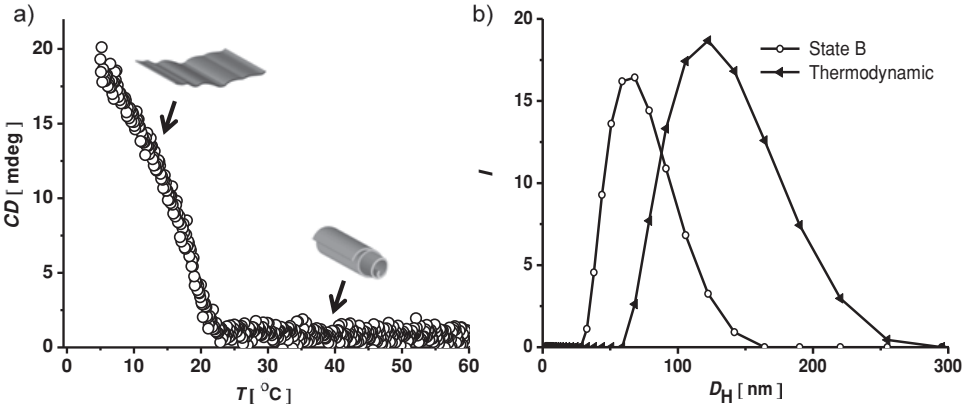

Figure 3. Annealing induced phase transition in **(S)-OPV-ch** ($c = 5 \times 10^{-5}$ M) self-assembly, in 10% THF/water solvent mixture: a) Temperature dependent cooling curve by monitoring the CD intensity at 415 nm ($-dT/dt = 2$ °C/min). b) DLS spectra of the assembly before (State B) and after (thermodynamic) annealing.

diameter of the **(S)-OPV-ch** is increased from 68 to 120 nm, with much broader distribution, upon annealing (Figure 3b). Accordingly, the microscopic analyses of the thermodynamically stable phases revealed the presence of only nanosheets, suggesting the opening up of nanotubes upon annealing.[16] At higher percentages of water, this phase can be directly achieved whereas at lower percentages an annealing process is required to attain them. Hence, it is evident that 2D sheets are the thermodynamically favoured phase for the OPV amphiphilic self-assembly, irrespective of the solvent composition. The phase transition from sheets to tubes can be explained by the fact that with higher percentages of THF the assembly is a folded tube, probably an attempt by the assembly to reduce the interfacial energy. However as the dielectric constant of the mixture increases (with increase in water percentage) the dipolar interactions of TEG chains decrease hence resulting in the opening of the structures forming sheets.[18]

Remarkably, the thermodynamically stable OPV nanosheets formed from different solvent compositions, showed only marginal changes in its size on further heating as evident from the DLS studies.[16] This suggests that the synergistic π–π interactions of the OPV segments and the hydrophobic interactions associated with amphiphilic interactions are very strong, thereby rendering the self-assembled sheets high stability. Moreover, these nanosheets formed at different solvent compositions exhibit a highly cooperative transition from excitonically coupled, ordered molecular organization to a less-ordered phase with increase in temperature. This transition can be spectroscopically probed by either the disappearance of CD signal or the vibrionic shoulder in the absorption spectrum.[16] For example, **Figure 4**a shows the temperature dependent CD spectra of **(S)-OPV-ch** (5×10^{-5} M) in 2.5% THF/water mixture, which showed the disappearance of CD signal above 46 °C accompanied by the disappearance of the vibrionic shoulder in the absorption spectrum. The corresponding temperature sweeps by monitoring the CD signal at 415 nm, suggests that this thermal transition is a highly cooperative process and is completely reversible (Figure 4b). However, DLS studies showed only marginal changes in the aggregate size with temperature, reiterating that this transition involves only molecular rearrangement and no melting of assemblies or rolling-up of the sheets occurs.[16] Since, molecular organization plays a crucial role in the performance of devices, we probed the factors which influence this transition temperature (T_t) in the OPV sheets. The transition occurred at higher temperatures with increasing concentration.[16] Moreover, T_t for **OPV-ach** assembly is found to be higher compared to **(S)-OPV-ch** at the same concentration.[16]

2.2.5. OFET Device Characteristics

Detailed studies of organic field-effect transistor (OFET) devices based on the self-assembled OPV structures as the transport layer were carried out. In general, all the OPV systems including the tubes and the sheets exhibited *p*-type transport. The supramolecular active layer was introduced directly from the solution phase on the dielectric layer forming top-contact, bottom-gated FET structures. Mobility (μ_{FET}) as high as 0.8×10^{-2} cm^2 V^{-1} s^{-1} was obtained for **OPV-ach** sheets with an average mobility of 5×10^{-3} cm^2 V^{-1} s^{-1} (obtained from a set of 10 devices) and current modulation on/off ratio $\approx 10^3$ (**Figure 5**a,b). On the other hand, sheets fabricated from **(S)-OPV-ch** also exhibited mobility of 7.5×10^{-3} cm^2 V^{-1} s^{-1}, suggesting that branched side chains do not influence the molecular organization to a great extent due to the strong hydrophobic interactions.[16] Remarkably, these mobility values of the OPV sheets are three orders of magnitude greater than reported for assemblies of OPVs and higher than many other chromophoric systems on a FET device.[12] Moreover, the mobility achieved is only marginally lower than the highest value obtained for vacuum-deposited OPV films.[6c] It is also noteworthy that FET mobilities of self-assembled chromophoric systems are lower, as expected, than the mobility values obtained from non-contact mode conductivity techniques.[5a]

Interestingly, transistors fabricated from the rolled-tubes of **OPV-ach** showed much lower mobilities ($\mu_{FET} = 1.03 \times 10^{-4}$ cm^2 V^{-1} s^{-1}) (Figure 5c,d).[16] This trend can be explained on the basis of both macroscopic and microscopic factors. Molecular organization resulting in the form of sheets is expected to have a better coverage in terms of occupying the entire area between the drain (D)–source (S) electrodes and ensuring a complete translation of gate voltage (V_g) to surface

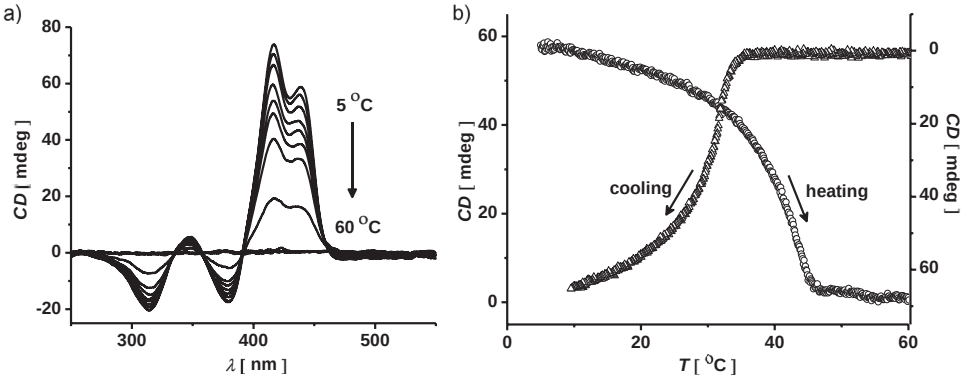

Figure 4. Temperature dependent phase transition in the **(S)-OPV-ch** sheets (5×10^{-5} M, 2.5% THF in water): a) Temperature dependent CD spectra while heating. b) Heating and cooling curves ($dT/dt = \pm 2$ °C/min) of the sheets by monitoring the CD signal at 415 nm, demonstrating the cooperative phase transition.

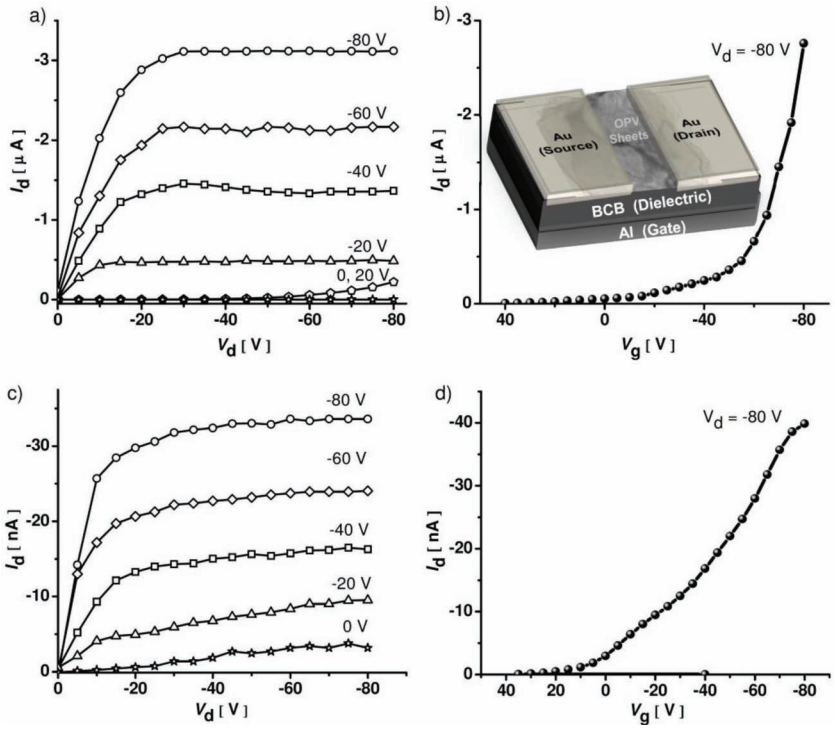

Figure 5. a,b) Typical output and transconductance curves for **OPV-ach** sheets in top contact bottom gate FET with L (channel length) ≈ 20 μm, W (channel width) ≈ 1 mm and C (capacitance per unit area of the gate insulator layer) ≈ 4 nF/cm^2. Inset of (b) shows the schematics of the device structure with OPV sheets as active layer. c,d) Typical output and transconductance curves for **OPV-ach** nanotubes in top contact bottom gate FET with L ≈ 20 μm, W ≈ 1 mm and C ≈ 4 nF/cm^2.

charges at the interfaces, while in case of a random assortment of tubes, the coverage is dependent on the packing fraction and is expectedly less dense. In case of tubes, the gate bias potential V_g does not get completely translated into interface charges, thereby reducing the estimated mobility. In case of an extended 2-dimensional microtube percolation network, the relationship between the percolation threshold (N_c) and tube length (L) takes the form, L $(\pi N_c)^{1/2} = 4.2$.[20] Applying this condition for the present case where the tubes have length ≈ 1 μm, a percolation threshold of ≈5 μm^{-2} is obtained. Since the film deposition was carried out by multiple drop-casting procedure from concentrated solution, it was ensured that we were above the percolation threshold for 1D transport. The density of OPV tubes in our device is ≈10 μm^{-2}. Mobility at a microscopic level then is a representative figure of merit of the electrical characteristics of individual tube and sheet. Mobility arrived from FET measurements can be used as an estimate of molecular packing upon assuming optimized filling. Comparison of charges induced on the sheet and tubes with C (capacitance per unit area of the gate insulator layer) ≈4 nF/cm^2 and V_g = –80 V gives an upper limit of the doping level (≈10^9 for rolled tubes and ≈10^{11} for sheets). From a microscopic perspective, the sheet formation involves growth along the π-stacking direction and uniform lamellar packing is obtained with slipped sheets at the dielectric-semiconductor interface. Higher degree of charge-carrier delocalization is expected in the 2-D sheet than the 1-D tube structures, along with a higher tolerance for defects in the 2D systems compared to 1D systems.[21] The enhanced electrical transport processes of the OPV-sheets can be attributed to a combination of these factors. In general however, higher mobility in these nanostructures can be due to the existence of strong π–π interactions, by virtue of the amphiphilic design, along the charge transport direction coupled with a higher degree of order.

3. Conclusions

In conclusion, we present here the unprecedented self- assembly of OPV amphiphiles into free standing, nanostructured sheets with high stability and structural order. Spectroscopic probing has provided insights into the molecular ordering in the OPV sheets as well as into different phases of the assembly. FET devices have been fabricated by direct solution processing of these supramolecular assemblies, with a clear distinction in mobility values for the tubes (1.03×10^{-4} cm^{2}V^{-1}s^{-1}) and sheets (8×10^{-3} cm^{2}V^{-1}s^{-1}, thermodynamic phase). More importantly, the mobility obtained for the OPV sheets (8×10^{-3} cm^2 V^{-1} s^{-1}) is one of the highest values reported for the self-assembled nanostructures of chromophores on a FET device structure. We envisage that the amphiphilic molecular design would be the key to obtaining self-assembled morphologies of higher structural order and hence better supramolecular device characteristics.

4. Experimental Section

Synthesis and Characterization: The OPV amphiphiles (**OPV-ach** and **(S)-OPV-ch**) were synthesized through a statistical Wittig–Horner reaction between the bisphosphonate (**6**)[16] and the respective aldehydes. The bisphosphonate (0.26 g, 0.64 mmoles) was taken in dry DMF (7 mL) under nitrogen atmosphere and stirred at room temperature till it dissolved completely. Potassium *t*-butoxide (0.23 g, 2.05 mmole) was then transferred under inert conditions and the reaction mixture was stirred for 10 min until it turned dark, indicating the formation of anions. The aldehydes (0.64 mmole each) were weighed separately, dissolved in dry DMF (5 mL) and were added to the reaction mixture drop wise. The reaction mixture was allowed to stir under N_2 atmosphere for additional 3 h. After the completion of the reaction, an extraction was done with water: diisopropyl ether. The organic layer was collected, dried over anhydrous Na_2SO_4 and was concentrated on a rotary evaporator. The crude mixture of **OPV-ach** and **(S)-OPV-ch** was purified by silica gel column chromatography and neutral alumina column chromatography (chloroform: methanol) respectively and then subjected to biobeads ($CHCl_3$, SX-3) to get **OPV-ach** and **(S)-OPV-ch** as yellow solids with the yields of 14.9% and 7.2%, respectively. The amphiphiles were obtained along with the bolaamphiphiles and the respective dialkyl substituted derivatives in the statistical reactions performed.

OPV-ach: ^{1}H NMR (400 MHz, $CDCl_3$, δ): 7.47 (d, J = 8.8 Hz, 4H, ArH), 7.34 (d, J = 16.4 Hz, 1H, vinylic H), 7.33 (d, J = 16.4 Hz, 1H, vinylic H), 7.10 (s, 2H, ArH), 7.06 (d, J = 16.4 Hz, 1H, vinylic H), 7.05 (d, J = 16.4 Hz, 1H, vinylic H), 6.91 (d, J = 8.8 Hz, 2H, ArH), 6.88 (d, J = 8.8 Hz,

2H, ArH), 4.16 (t, J = 5.2 Hz, 2H, OCH_2), 3.98 (t, J = 5.2 Hz, 2H, OCH_2), 3.91 (s, 6H, Ar OCH_3), 3.73 (m, 2H), 3.67 (m, 8H), 3.54 (m, 2H), 3.38 (s, 3H, TEG OCH_3), 1.78 (m, 2H), 1.5-1.2 (m, 20H), 0.89 (t, J = 6.4 Hz, 3H, CH_3); ^{13}C NMR (100 MHz, $CDCl_3$, δ): 158.9, 158.6, 151.6, 151.5, 132.1, 130.7, 128.6, 128.5, 127.9, 126.8, 126.7, 121.4, 121.2, 114.9, 109.2, 72.1, 71.0, 70.8, 70.7, 69.9, 68.2, 67.6, 59.2, 56.6, 29.8-29.7, 29.6-29.5, 26.2, 22.8, 14.3; MALDI-TOF-MS (m/z): calcd for $C_{45}H_{64}O_8$: 732.4601; found: 732.56 [M^+]; HRMS (ESI) m/z: [M]$^+$ calcd for $C_{45}H_{64}O_8$, 732.4601; found, 755.4499 [M+Na$^+$].

(S)-OPV-ch: ^{1}H NMR (400 MHz, $CDCl_3$, δ): 7.47 (d, J = 8.4 Hz, 4H, ArH), 7.34 (d, J = 16.4 Hz, 1H, vinylic H), 7.33 (d, J = 16.4 Hz, 1H, vinylic H), 7.11 (s, 2H, ArH), 7.06 (d, J = 16.4 Hz, 1H, vinylic H), 7.05 (d, J = 16.4 Hz, 1H, vinylic H), 6.91 (d, J = 8.8 Hz, 2H, ArH), 6.89 (d, J = 8.8 Hz, 2H, ArH), 4.15 (t, J = 5.2 Hz, 2H, OCH_2), 4.02 (m, 2H, OCH_2), 3.91(s, 6H, Ar OCH_3), 3.74 (m, 2H), 3.67 (m, 8H), 3.54 (m, 2H), 3.38 (s, 3H, TEG OCH_3), 1.78 (m, 2H), 1.9-0.8 (19H, alkyl H); ^{13}C NMR (100 MHz, $CDCl_3$, δ): 151.5, 130.7, 128.6, 128.4, 127.9, 126.6, 121.4, 121.2, 114.9, 114.8, 109.2, 109.1, 72.1, 71.0, 70.8, 70.7, 69.9, 67.7, 66.6, 59.2, 56.6, 39.4, 37.4, 36.4, 30.1, 28.1, 24.8, 22.8, 22.7,19.8; MALDI-TOF-MS (m/z): calcd for $C_{43}H_{60}O_8$: 704.4288; found: 704.39 [M^+]; HRMS (ESI) m/z: [M]$^+$ calcd for $C_{43}H_{60}O_8$, 704.4288; found, 727.4186 [M+Na$^+$].

Optical and Spectroscopic studies: AFM images shown in the main text were performed on a Veeco diInnova SPM operating in tapping mode regime. Micro - fabricated silicon cantilever tips doped with phosphorus and with a frequency between 235 and 278 kHz and a spring constant of 20-40 Nm^{-1} were used. AFM images shown in the supporting information were performed on JPK Nanowizard 3 instrument. Contact conducting cantilever tips made of Cr/Pt coated on Silicon and with a frequency between 13 to 15 kHz and a spring constant of 0.2 Nm^{-1} The samples were prepared by drop casting a solution of **OPV-ach** on a glass substrate and dried under high vacuum at room temperature. FE-SEM measurements were performed on a NOVA NANO SEM 600 (FEI) by drop casting the solutions on glass substrates followed by drying under high vacuum at room temperature and was operated with an accelerating voltage of 5 kV. TEM measurements were performed on a JEOL, JEM 3010 operated at 300 kV. Samples were prepared by placing a drop of the solution on carbon coated copper grids followed by drying at room temperature. The images were recorded with an operating voltage of 300 kV. In order to get a better contrast, the samples were stained with uranyl acetate (1 wt% in water) before the measurements. Confocal Microscopy imaging was done at room temperature using a Zeiss LSM 510 META laser scanning confocal microscope. The microscope objective of 63X (NA 1.4) and 20X (NA 0.5) were employed. A filter of ChS-1: 503-717 was used. Samples were prepared by sealing the solution between two glass plates. Electronic absorption spectra were recorded on a Perkin Elmer Lambda 900 UV-vis-NIR spectrometer and emission spectra were recorded on Perkin Elmer Ls 55 luminescence spectrometer. Fluorescence spectra of solutions were recorded by exciting the **OPV-ach** and **(S)-OPV-ch** at 380 and 310 nm respectively. Circular dichroism (CD) spectra and temperature dependent UV-vis spectra were recorded on a Jasco J-815 spectrometer where the sensitivity, time constant and scan rate were chosen appropriately. The temperature dependent measurements were performed with a CDF-426S/15 Peltier-type temperature controller with a temperature range of 263–383 K and adjustable temperature slope. NMR spectra were recorded with a Bruker AVANCE 400 (400 MHz) Fourier transform NMR spectrometer with chemical shifts reported in parts per million (ppm) with respect to TMS. Dynamic light scattering experiments measurements were carried out using a NanoZS (Malvern UK) employing a 532 nm laser at a back scattering angle of 173°. The samples were measured in a 10 mm glass cuvette. Small angle XRD patterns were recorded in Siefert XRD instrument using (Cobalt (Co)) source (θ = 0.4°–60°). Wide angle XRD patterns were recorded using (Copper Kα (Cu) source (θ = 2.5°–60°). MALDI-TOF spectra were obtained on a Brukerultraflex 2 MALDI-TOF mass spectrometer with α-cyano-4-hydroxycinnamic acid matrix. HRMS spectra were obtained with an ESI technique.

Field Effect Mobility Measurements: Field effect mobility measurements were performed on top contact bottom gate transistor structures. The fabrication of the field effect transistor (FET) involved coating of Al electrode (10^{-6} mbar, 40 nm thick) by physical vapor deposition on standard RCA treated cleaned glass substrates. This was followed by coating of the dielectric layer of hydroxyl free divinyl tetramethylsiloxane bis (benzocyclobutene) at 800 rpm for 1 min and annealed in a glove box atmosphere at 290 °C. The effective capacitance per unit area (C) of the dielectric films measured using Keithley 4200 semiconductor parameter analyser was obtained to be ≈4 nF/cm^2 for films of thickness 0.5–0.6 μm. The surface of the dielectric was further treated with hexamethyldisilazane in liquid by spin coating at 1500 rpm for 30 s and annealing at 110 °C for 2 h in N_2 atmosphere. This was followed by solution casting the thin film of the OPV assemblies in appropriate THF and water compositions to obtain films of thickness ≈300 nm. The source-drain Au electrode were also vapor deposited (10^{-6} mbar, 40 nm thick). The active layers were coated at different concentrations to distinctly follow the morphological changes with the transport measurements. The electrical characterization of the FETs were done using a standard set up of Keithley 2400 Source meters and a high impedance electrometer (Keithley 6514). The measurements were also cross checked with Keithley 2400 semiconductor parameter analyser.

The performance parameters of the devices were extracted in the saturation regime from the transconductance characteristics curves by using the equation: $I_{ds} = (\mu_{FET}WC/2L)\ (V_g - V_{th})^2$, where I_{ds} is the drain current, W and L are, respectively, the channel width and length, C is the capacitance per unit area of the gate insulator layer, and V_g and V_{th} are the gate voltage and the threshold voltage, respectively. The mobility values reported are the median value obtained from the measurements performed on 10–15 devices in each case which are representative of the general trends in these molecules.

Supporting Information

Supporting Information is available from the Wiley Online Library or from the author.

Acknowledgements

We thank Jawaharlal Nehru Centre for Advanced Scientific Research (JNCASR) and Department of Science and Technology (DST), Government of India for financial support. We thank Prof. G. U. Kulkarni (Veeco Lab), Dr. Basavaraj, Mr. Ashar, Mr. Prashant, (AFM), Mr. Piyush (DLS), Mrs. Usha (TEM), Miss. Selvi (FE-SEM) and Mr. Swamynathan (XRD, Raman Research Institute) for various measurements. B.N. and S.P.S. thank UGC for research fellowships.

Received: August 14, 2012
Revised: November 13, 2012
Published online: January 17, 2013

[1] a) F. Würthner, *Angew. Chem. Int. Ed.* **2001**, *40*, 1037–1039; b) F. J. M. Hoeben, P. Jonkheijm, E. W. Meijer, A. P. H. J. Schenning, *Chem. Rev.* **2005**, *105*, 1491–1546; c) A. P. H. J. Schenning, E. W. Meijer, *Chem. Commun.* **2005**, 3245–3258; d) A. C. Grimsdale, K. Müllen, *Angew. Chem. Int. Ed.* **2005**, *44*, 5592–5629.

[2] J. Roncali, *Chem. Rev.* **1992**, *92*, 711–738.

[3] a) R. E. Martin, F. Diederich, *Angew. Chem. Int. Ed.* **1999**, *38*, 1350–1377; b) J. M. Tour, *Chem. Rev.* **1996**, *96*, 537–553; c) *Electronic Materials: The Oligomer Approach* (Eds: K. Müllen, G. Wegner), Wiley-VCH, Weinheim **1997**.

[4] a) T. Aida, E. W. Meijer, S. I. Stupp, *Science* **2012**, *335*, 813–816; b) S. S. Babu, S. Prasanthkumar, A. Ajayaghosh, *Angew. Chem. Int. Ed.* **2012**, *51*, 1766–1776; c) A. Ajayaghosh, S. J. George, A. P. H. J. Schenning, *Top. Curr. Chem.* **2005**, *258*, 83–118;

d) F. Würthner, *Chem. Commun.* **2004**, 1564–1579; e) B.-K. An, J. Gierschner, S. Y. Park, *Acc. Chem. Res.* **2012**, *45*, 544–554.
[5] a) A. Saeki, Y. Koizumi, T. Aida, S. Seki, *Acc. Chem. Res.* **2012**, *45*, 1193–1202; b) M. Hasegawa, M. Iyoda, *Chem. Soc. Rev.* **2010**, *39*, 2420; c) T. Lei, J. Pei, *J. Mater. Chem.* **2012**, *22*, 785.
[6] a) C. D. Dimitrakopoulos, P. R. L. Malenfant, *Adv. Mater.* **2002**, *14*, 99–116; b) P. T. Herwig, K. Müllen, *Adv. Mater.* **1999**, *11*, 480–483; c) T. Yasuda, M. Saito, H. Nakamura, T. Tsutsui, *Appl. Phys. Lett.* **2006**, *89*, 182108.
[7] a) Y. Yamamoto, T. Fukushima, Y. Suna, N. Ishii, A. Saeki, S. Seki, S. Tagawa, M. Taniguchi, T. Kawai, T. Aida, *Science* **2006**, *314*, 1661–1663; b) H. J. Kim, T. Kim, M. Lee, *Acc. Chem. Res.* **2011**, *44*, 72–82; c) H. Shao, J. Seifert, N. C. Romano, M. Gao, J. J. Helmus, C. P. Jaroniec, D. A. Modarelli, J. R. Parquette, *Angew. Chem. Int. Ed.* **2010**, *49*, 7688–7857; d) C. Wang, Z. Wang, X. Zhang, *Acc. Chem. Res.* **2012**, *45*, 608–618; e) M. Kumar, S. J. George, *Chem. Eur. J.* **2011**, *17*, 11102–11106; f) K. V. Rao, K. Jayaramulu, T. K. Maji, S. J. George, *Angew. Chem. Int. Ed.* **2010**, *49*, 4218–4222.
[8] a) F. J. M. Hoeben, I. O. Shklyarevskiy, M. J. Pouderoijen, H. Engelkamp, A. P. H. J. Schenning, P. C. M. Christianen, J. C. Maan, E.W. Meijer, *Angew. Chem. Int. Ed.* **2006**, *45*, 1232–1236; b) X. Zhang, Z. Chen, F. Würthner, *J. Am. Chem. Soc.* **2007**, *129*, 4886–4887; c) K. V. Rao, S. J. George, *Org. Lett.* **2010**, *12*, 2656–2659; d) L. C. Palmer, S. I. Stupp, *Acc. Chem. Res.* **2008**, *41*, 1674–1684.
[9] a) W. J. Oldham Jr., R. J. Lachicotte, G. C. Bazan, *J. Am. Chem. Soc.* **1998**, *120*, 2987–2988; b) T. Goodson III, W. Li, A. Gharavi, L. Yu, *Adv. Mat.* **1997**, *9*, 639–643.
[10] a) J. H. Burroughes, D. D. C. Bradley, A. R. Brown, R. N. Masks, K. M. Mackay, R. H. Friend, P. L. Burns, A. B. Holmes, *Nature* **1990**, *347*, 539–541; b) M. Granstroöm, K. Petritsch, A. C. Arias, A. Lux, M. R. Andersson, R. H. Friend, *Nature* **1998**, *395*, 257–260; c) A. Kraft, A. C. Grimsdale, A. B. Holmes, *Angew. Chem. Int. Ed.* **1998**, *37*, 402.
[11] a) A. Ajayaghosh, A. V. Praveen, *Acc. Chem. Res.* **2007**, *40*, 644–656; b) D. G. Rodríguez, A. P. H. J. Schenning, *Chem. Mater.* **2011**, *23*, 310–325; c) A. Ajayaghosh, S. J. George, *J. Am. Chem. Soc.* **2001**, *123*, 5148–5149; d) A. P. H. J. Schenning, P. Jonkheijm, E. Peeters, E. W. Meijer, *J. Am. Chem. Soc.* **2001**, *123*, 409–416; e) G. N. Tew, M. U. Pralle, S. I. Stupp, *Angew. Chem. Int. Ed.* **2000**, *39*, 516–521.
[12] a) P. Jonkheijm, N. Stutzmann, Z. Chen, D. M. de Leeuw, E. W. Meijer, A. P. H. J. Schenning, F. Würthner, *J. Am. Chem. Soc.* **2006**, *128*, 9535–9540; b) M. Mas–Torrent, P. Hadley, P. Jonkheijm, A. P. H. J. Schenning, E. W. Meijer, S. George, A. Ajayaghosh, *J. Chem. Phys.* **2006**, *124*, 154704; c) Y. Yamamoto, G. Zhang, W. Jin, T. Fukushima, N. Ishii, A. Saeki, S. Seki, S. Tagawa, T. Minari, K. Tsukagoshi, T. Aida, *Proc. Nat. Acad. Sci. USA* **2009**, *106*, 21051–21056.
[13] a) S. Xiao, M. Myers, Q. Miao, S. Sanaur, K. Pang, M. L. Steigerwald, C. Nuckolls, *Angew. Chem. Int. Ed.* **2005**, *44*, 7390–7394; b) J. W. Chung, H. Yang, B. Singh, H. Moon, B.–K. An, S. Y. Lee, S. Y. Park, *J. Mater. Chem.* **2009**, *19*, 5920–5925.
[14] For self-assembled sheets from π-conjugated systems see; a) E. Lee, J. K. Kim, M. Lee, *Angew. Chem. Int. Ed.* **2009**, *48*, 3657–3660; b) J. Yin, Y. Zhou, T. Lei, J. Pei, *Angew. Chem. Int. Ed.* **2011**, *50*, 6320–6323; c) K. Liu, C. Wang, Z. Li, X. Zhang, *Angew. Chem. Int. Ed.* **2011**, *50*, 4952–4956; d) G. Fernández, F. García, F. Aparicio, E. Matesanz, L. Sánchez, *Chem. Commun.* **2009**, 7155–7157.
[15] Hulvat, M. F. Sofos, K. Tajima, S. I. Stupp, *J. Am. Chem. Soc.* **2005**, *127*, 366–372.
[16] See the Supporting Information.
[17] Twisted tubular phase has been isolated as the kinetic intermediate in self-assembled hexabenzocoronenes: T. Yamamoto, T. Fukushima, A. Kosaka, W. Jin, Y. Yamamoto, N. Ishii, T. Aida, *Angew. Chem. Int. Ed.* **2008**, *47*, 1672–1675.
[18] Y. Chen, B. Zhu, F. Zhang, Y. Han, Z. Bo, *Angew. Chem. Int. Ed.* **2008**, *47*, 6015–6018.
[19] L. Radzihovsky, J. Toner, *Phys. Rev. Lett.* **1995**, *75*, 4752–4755.
[20] L. Hu, D. S. Hecht, G. Gruner, *Nano Lett.* **2004**, *4*, 2513–2517.
[21] H. Sirringhaus, P. J. Brown, R. H. Friend, M. M. Nielsen, K. Bechgaard, B. M. W. L.-Voss, A. J. H. Spiering, R. A. J. Janssen, E. W. Meijer, P. Herwig, D. M. de Leeuw, *Nature* **1999**, *401*, 685–687.